International Journal of Power Electronics and Drive Systems (IJPEDS)
Vol. 12, No. 2, Jun 2021, pp. 943~956
ISSN: 2088-8694, DOI: 10.11591/ijpeds.v12.i2.pp943-956

Duty ratio control ofthree port isolated bidirectional asymmetrical triple active bridge DC-DC converter

Adarsh S., Nagendrappa H.
Department of Electrical and Electronics, National Institute of Technology Karnataka, Mangalore, India

Article Info

Article history:

Received Jan 2, 2021
Revised Feb 25, 2021
Accepted Mar 19, 2021

Keywords:

Bidirectional power flow
Duty ratio control
High frequency isolation
Switch utilisation
Zero voltage switching

ABSTRACT

Multiport converters are used in interfacing of distributed energy sources with grid/load. Isolated converters are needed in applications where converter gain is high and there is a requirement of isolation. Dual transformer asymmetric triple active bridge offers the advantage of reduced circulating current. However, the operating range is low for variation in load and source voltage. In this paper duty ratio modulation technique is proposed to regulate the load voltage and control the power flow in both the directions. As a result of the new gating scheme, the converter switches operate with ZVS, irrespective of variations in load power and source voltage. The converter is designed to ensure high switch utilization. The control technique is validatedthrough simulation of a 1kW three port DC-DC converter. It was observerd that the load voltage was regulated for wide range of variation in load power and source port voltages. The single input dual output mode was also verified.

Corresponding Author:

Adarsh S
Department of Electrical and Electronics Engineering
National Institute of Technology Karnataka, Surathkal
Dakshina Kannada District, Karnataka, India
Email: adarsh.srinivasaraghavan@gmail.com

1. INTRODUCTION

Multiport converters (MPC) are used in systems where more than two sources and loads are interfaced.The multiport converter has lower number of components compared to multiple two port converters; hence it is compact [1]-[3]. Multiport converters can be classified into three types based on the isolation of ports. They are, isolated, non-isolated and partially isolated MPC [2], [3]. In non-isolated MPC there is no galvanic isolation between any ports. Some ports of partially isolated MPC are isolated and all the ports are galvanically isolated in the case of Isolated MPC.

Isolated MPC is used in applications where there is a requirement of transformer isolation. It can also be used in applications demanding high converter gain and high power. Usually high frequency (HF) transformers are used in MPC, due to high switching frequency. This reduces the size of the transformer and other magnetic components [2]-[4]. Isolated MPC topologies have been derived from corresponding two port topologies, such as, forward converters, push-pull converters and flyback converters [2], [3].

Among the topologies reported in the literature, triple active bridge (TAB) has been researched extensively. It facilitates bidirectional power flow in all the ports [5]-[12]. The phase shift was optimized to minimize switching loses and mitigate electromagnetic issues [13]. Power flow was controlled using phase shift control method. The soft switching operating region with phase shift control was very narrow, hence duty ratio technique was utilized to increase the range of ZVS for variation of input voltage and load [14]-[18]. It also helped to reduce the switch voltage and current stresses. The topology is also scalable to higher ports.

[19]-[21] had demonstrated the scalability by extending the number of ports to four. However control of power flow in the topology involved cross coupling of control loops, this problem was rectified by the decoupling network implemented in [18]. LC, LLC and CLLC resonant tank circuits respectively were added to TAB converter, thereby reducing the switching losses and enabling the operation at 100 kHz, hence increasing the power density [22]-[24]. Two modules of TAB wereused to interface four ports, consisting of two energy storage devices. There was one energy storage device for each module and the source and loads were shared by both modules [25]. Distributed transformers were usedto reduce the input current ripples and included a decoupling networkin the control system to overcome the cross coupling [25]. Modified TAB with DCM operation ensured the decoupling operation by average current control, without the decoupling network [26]. Altering the geometry ofthe transformer core andwindings to obtain four quadrant integrated transformer structure resulted in decoupled control [27].

The topologies discussed earlier used three winding transformer, which is susceptible to magnetic short circuit [28]. To overcome this problem, dual transformer based topologies were implemented. They were multiport CLL resonant converter and Dual transformer asymmetrical triple active bridge (DTATAB). Multiport CLL resonant converter reduced the voltage stress in the switches; however, the load port was not bidirectional [29]. DTATAB ensured bidirectional power flow in all its ports, however its switch current and voltage stress were high [28]. Since only phase shift control was used to control the power flow, the switches did not operate with ZVS for the entire range of load and supply voltage. Hence, a new modulation technique (Duty ratio control) is proposed in this paper, to regulate load voltage, control power flow in both the directions and operate the switches with ZVS for the entire range of variation in the load and supply voltage.

The paper is organized as follows: working principle of duty ratio control applied to DTATAB topology is explained in Section 2. Steady state analysis is explained in Section 3. The converter design is given in Section 4 and the simulation results are discussed in Section 5. The conclusions are drawn in Section 6.

2. OPERATING PRINCIPLE

2.1. Circuit description

DTATAB is a dual transformer fully isolated three port converter. This configuration was initially implemented by Jakka *et. al.* to overcome the problems of magnetic short circuiting in the triple active bridge three port converter [28].

In this topology two voltage source ports are connected across two single phase H bridge inverters. The resistive load port is connected across a three phase inverter bridge. The transformers are connected to the bridge conFigureurations as shown in Figure 1. The switches of the individual inverters are gated in such a way as to control the phase shift between the inverter output voltages. By adjusting the phase shift between the transformer winding input voltages (inverter output voltages) the power delivered by the ports can be controlled and the load port voltage V_3 can also be regulated. This is called phase shift control. The process of controlling the pulse width of the transformer winding voltage waveforms (inverter output) is called duty ratio control. Using duty ratio control combined with phase shift control, it is possible to operate the converter switches with ZVS. Hence this work is aimed at applying a gating scheme in the switches to enable duty ratio control.

2.2. Gating scheme

V_1 and V_2 are DC voltage sources connected across port 1 and port 2 respectively, R is a resistive load connected across port 3. The capacitor C_3 is assumed to be large enough to obtain a DC voltage V_3 across R, with minimum ripple. The switches are gated as shown in Figure 2. The waveforms of inverter output voltages due to this gating scheme are as shown in Figure 2. The transformer winding currents are also shown in Figure 3.

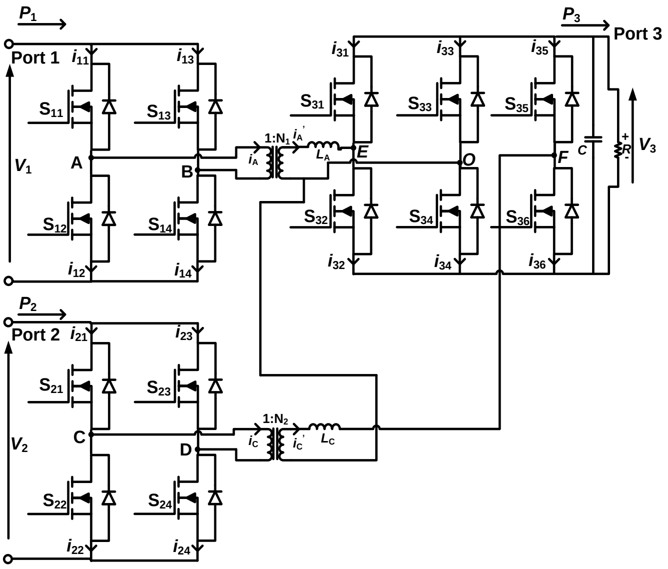

Figure 1. Circuit diagram of DTATAB

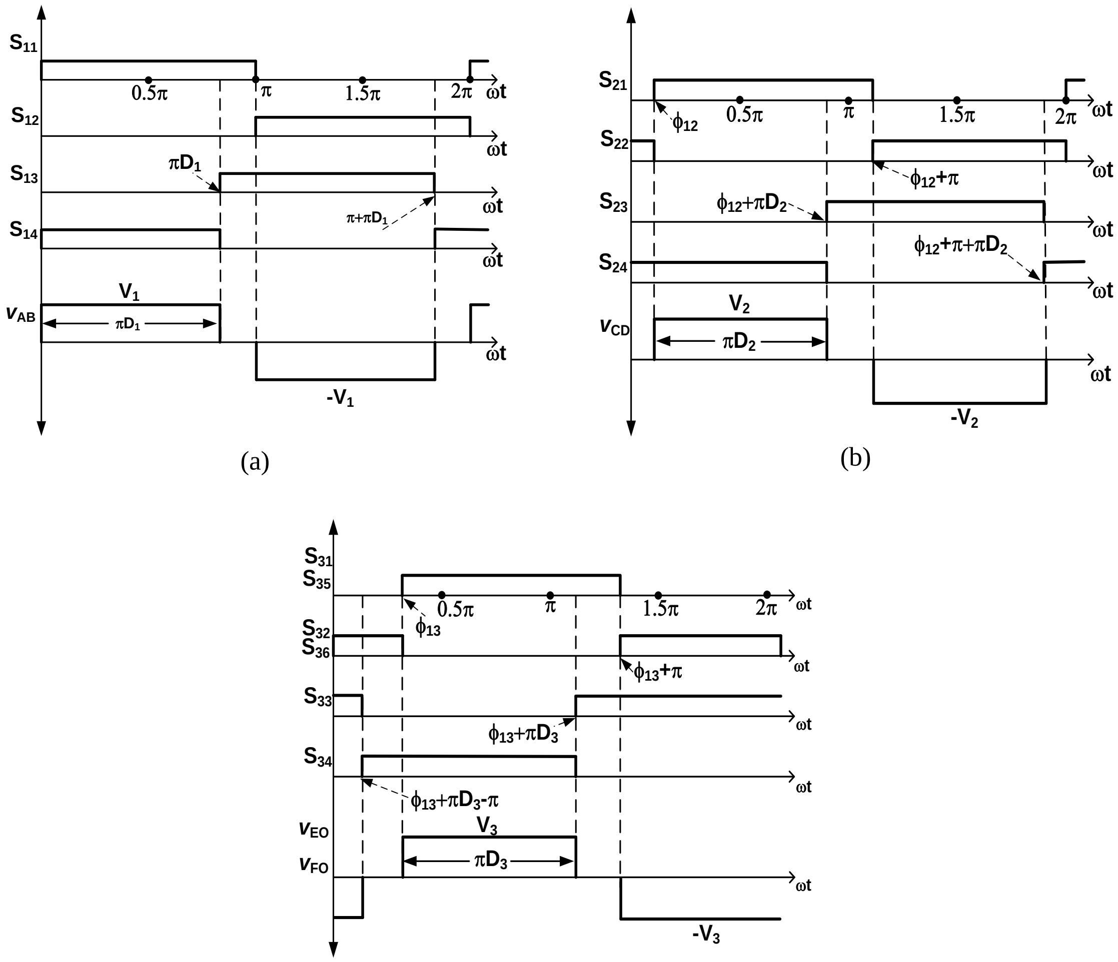

(a) (b)

(c)

Figure 2. (a) Gating signals of inverter interfacing port, (b) Gating signals of inverter interfacing port, (c) Gating signals of inverter interfacing port 3

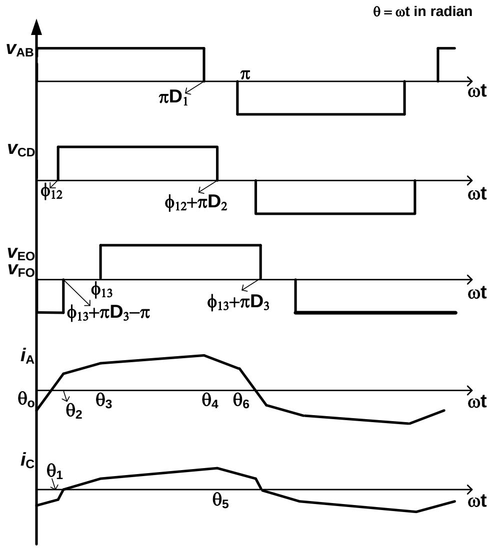

Figure 3. Inverter output voltages and transformer winding currents

2.3. Operation modes

There are six operating modes for half the switching cycle. The proposed modulation technique is symmetric.

a. Mode *1*:$\theta_0<\omega t<\theta_1$

S_{11}, S_{14}, S_{22}, S_{23}, S_{33}, S_{32}, S_{36} are the switches gated during this mode. The path of current flow is shown in Figure 4 (a). The voltage across A and B is (v_{AB}) is V_1, voltage across C and D is (v_{CD}) is V_2, the voltage across E and O (v_{EO}) and the voltage across F and O is (v_{FO}) is V_3. The winding currents are as shown in Figure 4 (a). The switch currents i_{s11} and i_{s14} are equal to i_A. Currents i_{s23} and i_{s22} are equal to -i_C. The currentsi_A and i_C are transformed as i_A and i_C in the secondary side of the transformer.The switch current i_{s32} is equal to i_A, is i_{s36} is equal to i_C and i_{s33} is equal to $i_{A'}+i_{C}$.

b. Mode 2$\theta_1<\omega t<\theta_2$

S_{11}, S_{14}, S_{22}, S_{24}, S_{33}, S_{32}, S_{36} are the switches gated during this mode. The path of current flow is shown in Figure 4(b). The voltage v_{AB} is V_1, vCD is 0, v_{EO} is V_3 and v_{FO} is V_3. The switch currents i_{s11} and i_{s14} are equal to i_A. Currenti_{s22} is equal to $-i_C$ and i_{s24} is equal to i_C. The switch current i_{s32} is equal to i_A, is i_{s36} is equal to $i_{C'}$and i_{s33} is equal to $i_{A'}+i_{C}$.

c. Mode 3: $\theta_2<\omega t<\theta_3$

S_{11}, S_{14}, S_{22}, S_{24}, S_{32}, S_{34}, S_{36} are the switches gated during this mode. The path of current flow is shown in Figure 4 (c). The voltage v_{AB} is V_1, vCD is 0, v_{EO} is 0 and v_{FO} is 0. The switch currents i_{s11} and i_{s14} are equal to i_A. Currents i_{s22} is equal to -i_C and $i_{s24}$is equal to i_C. The switch current i_{s32} is equal to i_A, i_{s36} is equal to $i_{C'}$ and i_{s34} is equal to $-(i_{A'}+i_{C'})$.

d. Mode 4: $\theta_3<\omega t<\theta_4$

S_{11}, S_{14}, S_{21}, S_{24}, S_{32}, S_{34}, S_{36} are the switches gated during this mode. The path of current flow is shown in Figure 4(d). The voltage v_{AB} is V_1, v_{CD} is V_2, v_{EO} is 0 and v_{FO} is 0. The switch currents i_{s11} and i_{s14} are equal to i_A. Currents i_{s21} and i_{s24} are equal to i_B. The switch current i_{s32} is equal to $i_{A'}$, is$_{36}$ is equal to i_C and $i_{s34}$is equal to $-(i_{A'}+i_{C'})$.

e. Mode 5: $\theta_4<\omega t<\theta_5$

S_{11}, S_{14}, S_{21}, S_{24}, S_{31}, S_{34}, S_{35} are the switches gated during this mode. The path of current flow is shown in Figure 4 (e). The voltage v_{AB} is V_1, vCD is V_2, v_{EO} is V_3 and v_{FO} is V_3. The switch currents i_{s11} and i_{s14} are equal to i_A. Currents i_{s21} and i_{s24} are equal to i_C. The switch current i_{s31} is equal to -i_A, is$_{35}$ is equal to -$i_{C'}$ and i_{s34} is equal to -$(i_{A'}+i_{C'})$.

f. Mode 6: $\theta_5<\omega t<\theta_6$

S_{11}, S_{13}, S_{21}, S_{24}, S_{31}, S_{34}, S_{35} are the switches gated during this mode. The path of current flow is shown in Figure 4 (f). The voltage v_{AB} is 0, v_{CD} is V_2, v_{EO} is V_3 and v_{FO} is V_3. The switch current i_{s11} is equal to i_A and i_{s13} is equal to -i_A. Currents i_{s21} and i_{s24} are equal to i_C. The switch current i_{s31} is equal to -i_A, is$_{35}$ is equal to -$i_{C'}$ and i_{s34} is equal to -$(i_{A'}+i_{C'})$.

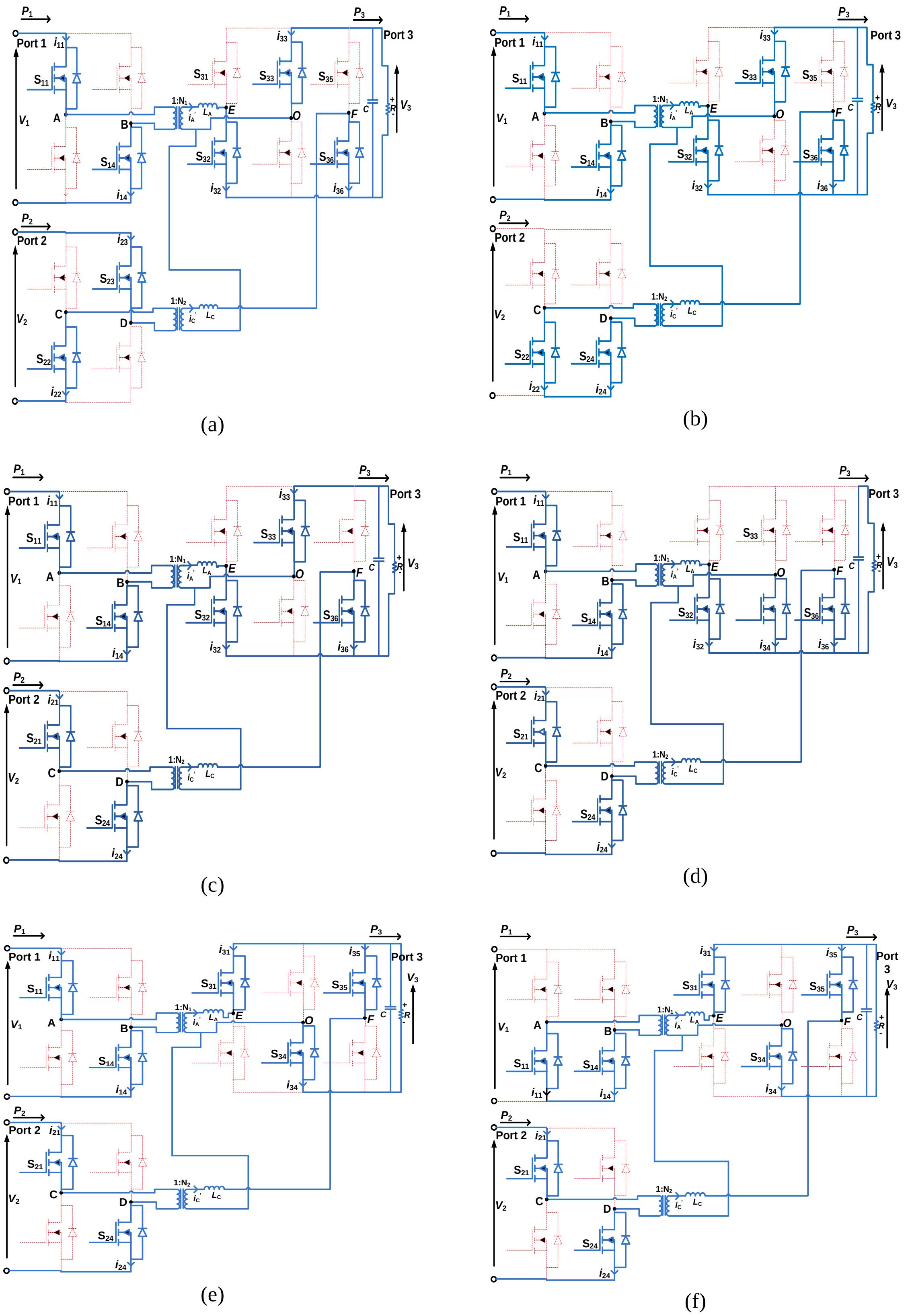

Figure 4. Converter current path and switching transition in (a) mode 1 (b) mode 2 (c) mode 3 (d) mode 4(e) mode 5 (f) mode 6

2.4. Equivalent circuit

Referring to the operation stages explained in Section II C, the circuit can be approximated to an equivalent circuit as shown in Figure 5. The following assumptions are made to obtain the equivalent circuit. L_1 and L_2 are the sum of the leakage inductance of the respective transformers referred to the secondary side and the inductors L_A and L_C respectively.

a. The switches and diodes are assumed to be ideal
b. The transformer can be replaced by a T equivalent circuit with all quantities referred to the secondary side
c. The transformer loses are neglected
d. The magnetizing inductance of the transformer can be neglected as its effect on the currents obtained will be minimum due to high switching frequency
e. All the switches in the converter are switched at the same switching frequency.

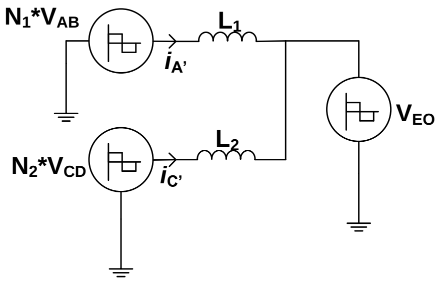

Figure 5. Equivalent circuit of DTATAB

3. STEADY STATE ANALYSIS

The current expressions for $i_{A'}$ and $i_{C'}$ are derived from the equivalent circuit using superposition theorem. There are 6 operating modes based on the values of phase shifts ϕ_{12}, ϕ_{23} and duty ratios D_1, D_2 and D_3. The voltage across port 3 can be expressed as shown in (1).

$$V_3 = \frac{n_1 R}{\omega L_1} M_{13} V_1 + \frac{n_2 R}{\omega L_2} M_{23} V_2 \quad (1)$$

the power at the three ports P_1, P_2 and P_3 can be expressed as shown in (2).

$$P_3 = \frac{n_1}{\omega L_1} M_{13} V_1 V_3 + \frac{n_2}{\omega L_2} M_{23} V_2 V_3 \quad (2)$$

$$P_1 = \frac{n_1}{\omega L_1} M_{13} V_1 V_3 \quad (3)$$

$$P_2 = \frac{n_2}{\omega L_2} M_{23} V_2 V_3 \quad (4)$$

$$where\ n_1 = \frac{1}{N_1}\ and\ n_2 = \frac{1}{N_2} \quad (5)$$
$$\omega = 2\pi f,$$

Where f is the switching frequency M_{13} and M_{23} depend on the phase shifts and duty ratios. Table 1 and Table 2 shows the expression of M_{13} and M_{23} respectively. For negative value of ϕ_{13}andϕ_{23}respectivelyM_{13} and M_{23} can be obtained by negating the corresponding expressions in Tables 1 and 2. The plots of M_{13} versus phase shift is shown in Figure 6. It can be observed from Figure 6 that M_{13} is maximum for phase shift of 90^o. Hence powertransferred is maximum at a phase shift of 90 ^{o}. Hence the phase shift is fixed at $90^o$and the power flow is controlled by varying the duty ratio D_1, D_2 and D_3. If D_3 is fixed at 1 and phase shift ϕ_{13} and $\phi_{23}$are fixed at $0.5\pi^c$, the value of M_{13} and M_{23} will depend on D_1 and D_2 alone, respectively. Since P_1 is proportional to M_{13} it can be controlled using D_1 and P_2 can be controlled using D_2 as it is proportional to M_{23} .Hence the technique is easy to implement.

Table 1. Expression of M13

Range of duty ratio D_1 and D_3	Expression of M_{13}
$D_3+\frac{\varphi_{13}}{\pi}\le D_1\le 1$ $0\le D_3\le 1-\frac{\varphi_{13}}{\pi}$	$\frac{\pi {D_3}^2}{2}+\frac{D_3\varphi_{13}}{2}-\frac{\pi D_1 D_3}{2}$
$\frac{\varphi_{13}}{\pi}\le D_1\le D_3+\frac{\varphi_{13}}{\pi}$ $0\le D_3\le 1-\frac{\varphi_{13}}{\pi}$	$\frac{-\pi {D_1}^2}{2}+D_1\varphi_{13}+\frac{\pi D_1 D_3}{2}-\frac{{\varphi_{13}}^2}{2\pi}$
$\frac{\varphi_{13}}{\pi}\le D_1\le 1$ $1-\frac{\varphi_{13}}{\pi}\le D_3\le 1$	$\varphi_{13}(1+D_1-D_3)-\frac{{\varphi_{13}}^2}{\pi}-\frac{\pi}{2}\{{D_1}^2-D_1D_3+(1-D_3)^2\}$
$0\le D_1\le \frac{\varphi_{13}}{\pi}+D_3-1$ $1-\frac{\varphi_{13}}{\pi}\le D_3\le 1$	$\frac{\pi {D_1}^2}{2}+\pi D_1-D_1\varphi_{13}-\frac{\pi D_1 D_3}{2}$
$0\le D_1\le \frac{\varphi_{13}}{\pi}$ $0\le D_3\le 1-\frac{\varphi_{13}}{\pi}$	$\frac{\pi D_1 D_3}{2}$
$1-\frac{\varphi_{13}}{\pi}\le D_3\le 1$ $D_3+\frac{\varphi_{13}}{\pi}-1\le D_1\le \frac{\varphi_{13}}{\pi}$	$\pi D_3+\frac{\pi D_1 D_3}{2}-\frac{\pi}{2}-\frac{\pi {D_3}^2}{2}-\frac{{\varphi_{13}}^2}{2\pi}-D_3\varphi_{13}$

Table 2. Expression of M_{23}

Range of duty ratio D_2 and D_3	Expression of M_{23}
$D_3+\frac{\varphi_{23}}{\pi}\le D_2\le 1$ $0\le D_3\le 1-\frac{\varphi_{23}}{\pi}$	$\frac{\pi {D_3}^2}{2}+\frac{D_3\varphi_{23}}{2}-\frac{\pi D_2 D_3}{2}$
$\frac{\varphi_{23}}{\pi}\le D_2\le D_3+\frac{\varphi_{23}}{\pi}$ $0\le D_3\le 1-\frac{\varphi_{23}}{\pi}$	$\frac{-\pi {D_2}^2}{2}+D_2\varphi_{23}+\frac{\pi D_2 D_3}{2}-\frac{{\varphi_{23}}^2}{2\pi}$
$\frac{\varphi_{23}}{\pi}\le D_2\le 1$ $1-\frac{\varphi_{23}}{\pi}\le D_3\le 1$	$\varphi_{23}(1+D_2-D_3)-\frac{{\varphi_{23}}^2}{\pi}-\frac{\pi}{2}\{{D_2}^2-D_2D_3+(1-D_3)^2\}$
$0\le D_2\le \frac{\varphi_{23}}{\pi}+D_3-1$ $1-\frac{\varphi_{23}}{\pi}\le D_3\le 1$	$\frac{\pi {D_2}^2}{2}+\pi D_2-D_2\varphi_{23}-\frac{\pi D_2 D_3}{2}$
$0\le D_2\le \frac{\varphi_{23}}{\pi}$ $0\le D_3\le 1-\frac{\varphi_{23}}{\pi}$	$\frac{\pi D_2 D_3}{2}$
$1-\frac{\varphi_{23}}{\pi}\le D_3\le 1$ $D_3+\frac{\varphi_{23}}{\pi}-1\le D_2\le \frac{\varphi_{23}}{\pi}$	$\pi D_3+\frac{\pi D_2 D_3}{2}-\frac{\pi}{2}-\frac{\pi {D_3}^2}{2}-\frac{{\varphi_{23}}^2}{2\pi}-D_3\varphi_{23}$

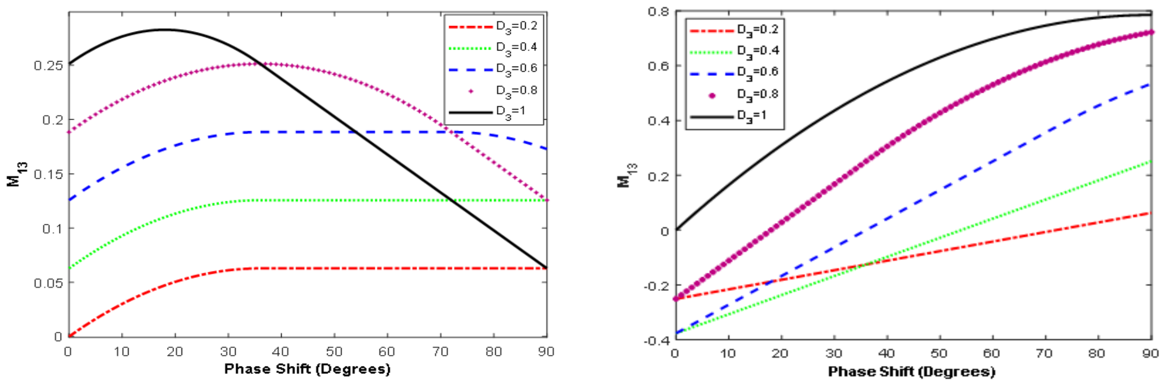

(a) (b)

Figure 6. Plot of M13vs phase shift for (a) D1=1 (b) D1=0.2

$when\ D_x\ge 0.5$

$$M_{x3} = \pi D_x - \frac{\pi^2}{4} - \frac{\pi}{2} D_x{}^2 \quad (5)$$

$$when\ D_x < 0.5$$
$$M_{x3} = \frac{\pi}{2} D_x{}^2 \quad (6)$$
$$where\ x\ is 1\ for\ port\ 1\ and\ 2\ for\ port\ 2$$

The plot of M_{13} versus D_1 is shown in Figure 7. The graph of M_{23} versus D_2 is same as Figure 7.

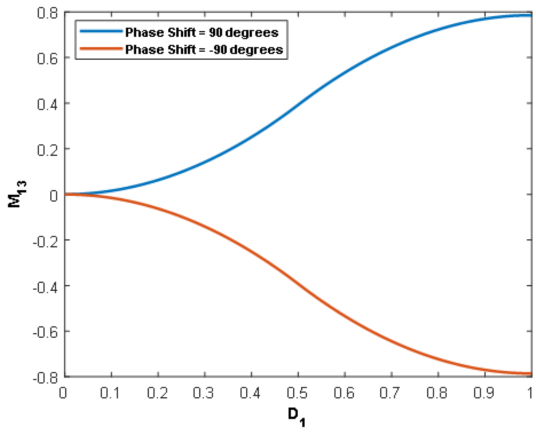

Figure 7. Gain vs Duty Ratio at Phase Shift 90o and -90o

For both the cases the expression of current in the switches during turn on is given by (7).

$$i_x(0) = -\frac{1}{wL}\left[\left(nV_x \frac{\pi D_x}{2}\right)\right] \quad (7)$$

Since (7) is negative irrespective of V_x and D_x it can be inferred that the converter switches operate with ZVS irrespective of load power and source voltage variations. However, in the case of standalone phase shift control, ZVS can occur only when the condition specified in (8) is satisfied. Hence when the range of ZVS is taken into consideration, duty ratio control is better than phase shift control.

$$V_3 - nV_x \leq 0c \quad (8)$$

4. DESIGN

In this section an isolated DTATAB DC to DC Converter is designed for the specifications given in Table 3, the converter is designed for worst case operating conditions of minimum voltage in port 1, port 2 and maximum load of 1KW. It is a desirable quality to design the converter in such a way as to increase the switch utilization. Switch utilization defined by (9).

$$U = \frac{P_3}{S} \quad (9)$$

where P_3 is the maximum power at port 3 (Load power) and S is the switch stress given by (10).

$$S = \sum_{x=1}^{4} V_{S_{1x(max)}} I_{S_{1x(max)}} + \sum_{x=1}^{4} V_{S_{2x(max)}} I_{S_{2x(max)}} + \sum_{x=1}^{6} V_{S_{3x(max)}} I_{S_{3x(max)}} \quad (10)$$

$$S = 4\left\{\left[\left(\frac{V_1}{n} + V_3\right) \times \left(I_{13_{max}}\right)\right] + \left[\left(\frac{V_2}{n} + V_3\right) \times \left(I_{23_{max}}\right)\right]\right\} \quad (11)$$

From Figure 8 (Left) it can be understood that the switch utilization is maximum when $P_2=(V_2/V_1)*P_1$. The ratio of power between port 2 and port 1 is fixed at (V_2/V_1), as it cannot be increased further. Switch utilization is plotted versus n/ (ω*L) for different values of transformer turns ratio in Figure 8

(Right). It is observed in the plot that utilization increases with increase in transformer turns ratio and reduction in inductance. Hence $n=n_1=n_2$ is chosen as 5 and n/ (ω*L) is chosen as 0.1768. Hence the inductance $L_1=L_2=L$ is 45μH. In (1) can be modified as shown in (12).

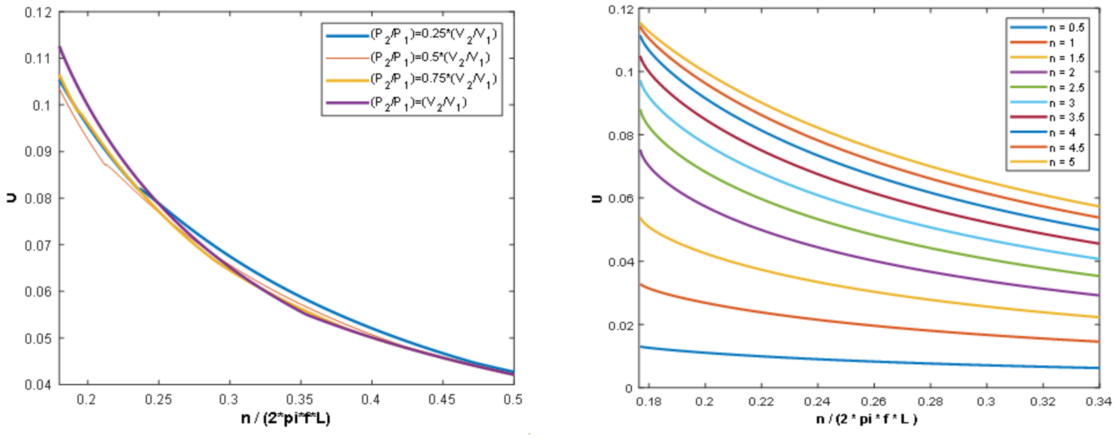

Figure 8. Switch Utilisation (U)vs n/(2*π*f *L) for different values of P2/P1(Left) and different values of n (Right)

Table 3. Converter specifications

V_1 (V)	V_2 (V)	V_3 (V)	Switching Frequency f (KHz)	P_3 (KW)
48 to 72	24 to 48	100	100	1

$$V_3 = \frac{n}{\omega L} R\, V_1 M_{13} \left(1 + \frac{P_2}{P_1}\right) \tag{12}$$

substituting the values of $n, \frac{P_2}{P_1}$ *and* L

$$M_{13} = \frac{2\times\pi\times 100kHz\times 45\mu H}{10\times 48\times\left(1+\frac{24}{48}\right)} = \frac{\pi}{4} \tag{13}$$

Dividing (4) by (3), (14) is obtained.

$$\frac{P_2}{P_1} = \frac{M_{23}V_2}{M_{13}V_1} \tag{14}$$

$$M_{23} = M_{13} = \frac{\pi}{4} \tag{15}$$

D1 and D2 are deduced from Figure 7.

$$D_1 = D_2 = 1 \tag{16}$$

The converter parameter design values are displayed in Table 4

Table 4. Converter Parameter design values

R (Full Load) (Ω)	n	L (μH)	ϕ_{13}	ϕ_{23}	D_1	D_2	D_3
10	5	45	$0.5\pi^c$	$0.5\pi^c$	1	1	1

5. RESULTS

In this section, the simulation results of a 1KW DTATAB DC-DC converter designed in Section 4 is shown. The worst case operating condition is V_1=48V, V_2=24V and the load R=10Ω. Both the ports 1 and 2 deliver equal power to port 3. For changes in load connected to port 3, V_3 is regulated to 100V by adjusting the duty ratios D_1 and D_2.

The converter is simulated in PSIMto verify load voltage regulation (port 3) and ZVS in all the converter switches for different values of load (R, connected at port 3) and voltages at port 1(V_1) and port 2(V_2) .The value of load voltage, calculatedtheoriticaly (Th) and obtained through simulation (Sim) is tabulated in Table 5 and average current delivered by port 1 is tabulated in Table 6, forvarying valuesof load and source voltages in port1 and port 2. The average current delivered by port 2 is same as port 1. From Table 5, it is evident that the load voltage (V_3) is regulated at 100V, irrespective of variations in source voltage V_1, V_2 and load R. The ratio of P_2 to P_1 ismaintained at $V_2/V_{1,}$ to maximise the switch utilisation.

Figure 9 and Figure 10 show the waveforms of switch currents through all the converter switches, for full load. It can be observed from the waveformsthat every switch is turned on with ZVS. Hence, the switching losses are reduced in the converter due to soft switching. As the load reduces, the duty ratio D_1 and D_2 are reduced to regulate the load voltage V_3, keeping D_3, ϕ_{13} and ϕ_{23} constant. Hence the converter operates with mode 3 or mode 4. In mode 3 or mode 4 the switch operates with ZVS irrespective of port voltages or load value. To demonstrate ZVS at a lower value of load, the switch current waveforms for 10% of full load are shown in Figure 11 and Figure 12. It is evident from the switch current waveforms in Figure 11 and Figure 12 that all the converter switches turn on with ZVS.

The results mentioned earlier in this section correspond to the dual input single output case. The waveforms of load voltage, source currents and transformer winding voltages at 50% of full load are shown in Figure 13 (a).The figure shows that the load voltage is regulated at 100V and the source currents I_1 and I_2 are equal, which indicates that the ratio of P_2 to P_1 ismaintained at V_2/V_1.As the converter has bidirectional capability, it can operate in single input dual output mode, with port 1 being the input port and port 2, port 3 being the load ports.The simulation is performed to verify whether V_2 is regulated at 24V and V_3 is regulated at 100V, when port 3 and port 2 are loaded to 500W and 100W respectively. The voltages at port 2 and port 3 are regulated by adjusting D_1 at 0.7764, D_2 at 0.3873, ϕ_{13} at $0.5*\pi$ and ϕ_{23} at $-0.5*\pi$. The waveforms of load voltage, source currents and transformer winding voltages in the single input dual output mode are shown in Figure 13 (b). The figure shows that the value of V_2 and V_3 are 24V and 100V respectively, hence the voltage regulation is verified.

The results demonstrate the capability of duty ratio control to regulate the load voltage effectively for wide range of variation in load and source voltages. It is also shown that the converter switches operate with ZVS irrespective of the load and source voltage value. The bidirectional operation is verified from a case of single input dual output operation.

Table 5. Simulation results: average value of V3

Sl No	V_1 (V)	V_2 (V)	R (Ω)	D_1	D_2	V_3 (V)	
						Th	Sim
1.	48	24	10	1	1	100	100.45
2.	48	24	20	0.5	0.5	100	100.31
3.	48	24	100	0.22	0.22	100	100.19
4.	72	24	10	0.65	0.65	100	100.36
5.	48	48	10	0.65	0.65	100	100.28
6.	72	48	10	0.55	0.55	100	100.37

Table 6. Simulation results: average value of I1

Sl No	V_1 (V)	V_2 (V)	R (Ω)	D_1	D_2	I_1 (A)	
						Th	Sim
1.	48	24	10	1	1	13.89	13.91
2.	48	24	20	0.5	0.5	6.94	6.94
3.	48	24	100	0.22	0.22	1.39	1.37
4.	72	24	10	0.65	0.65	10.42	10.54
5.	48	48	10	0.65	0.65	10.42	10.61
6.	72	48	10	0.55	0.55	8.33	8.40

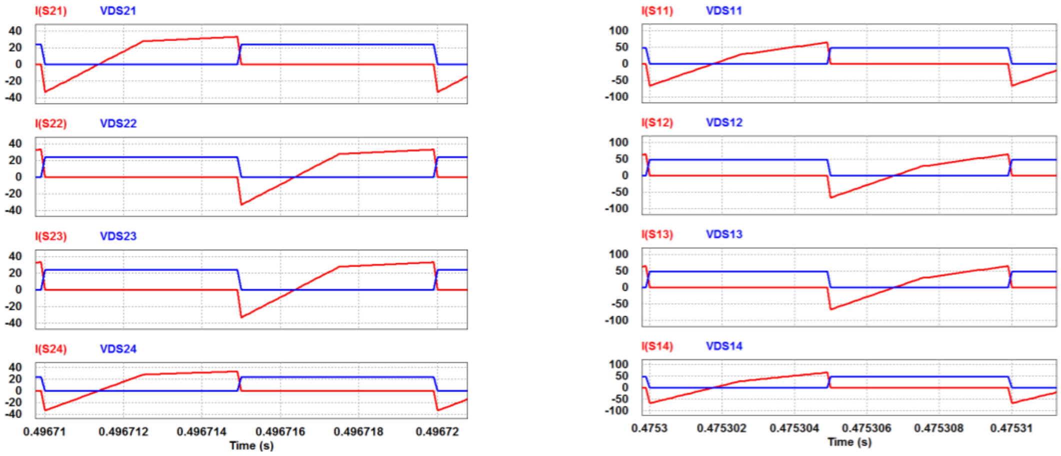

(a) (b)

Figure 9. Switch currentand voltage waveforms in (a) AB interfacing port 1 (b) AB interfacing port 2, for 100% load

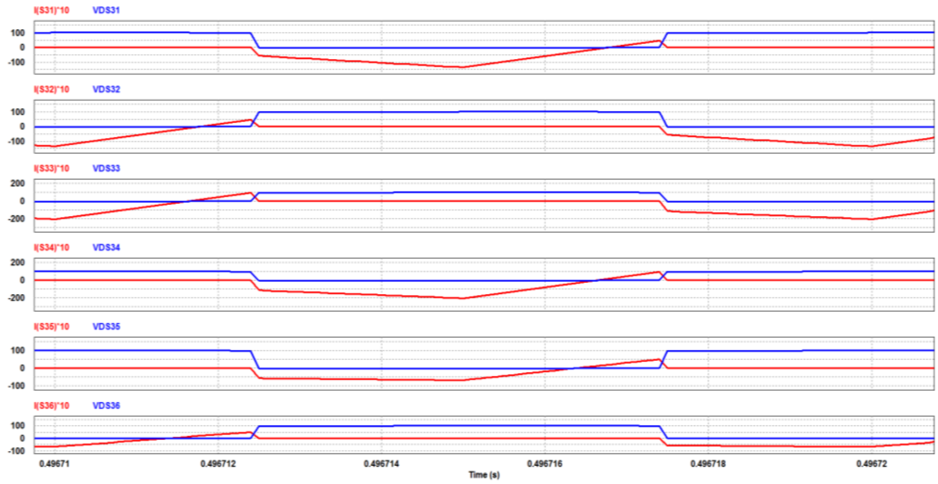

Figure 10. Switch current and voltage waveforms AB interfacing port 3, for 100% load

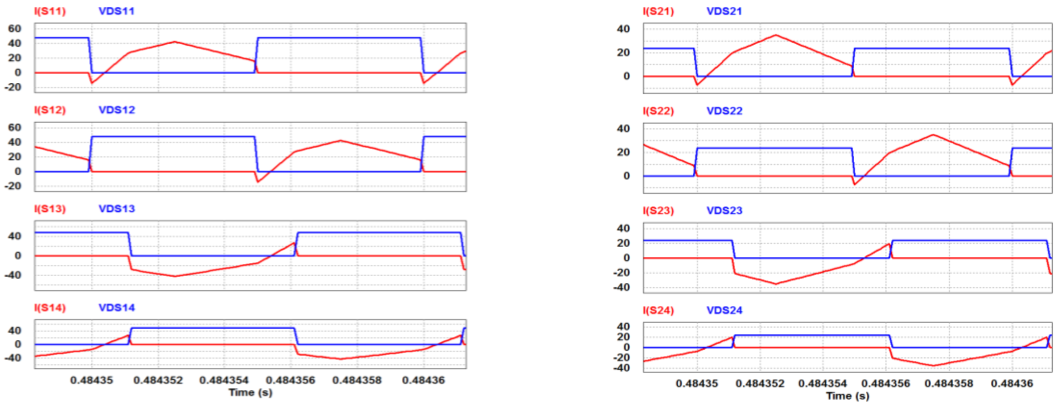

(a) (b)

Figure 11. Switch currentand voltage waveforms in (a) AB interfacing port 1 (b) AB interfacing port 2, for 10% of Full load

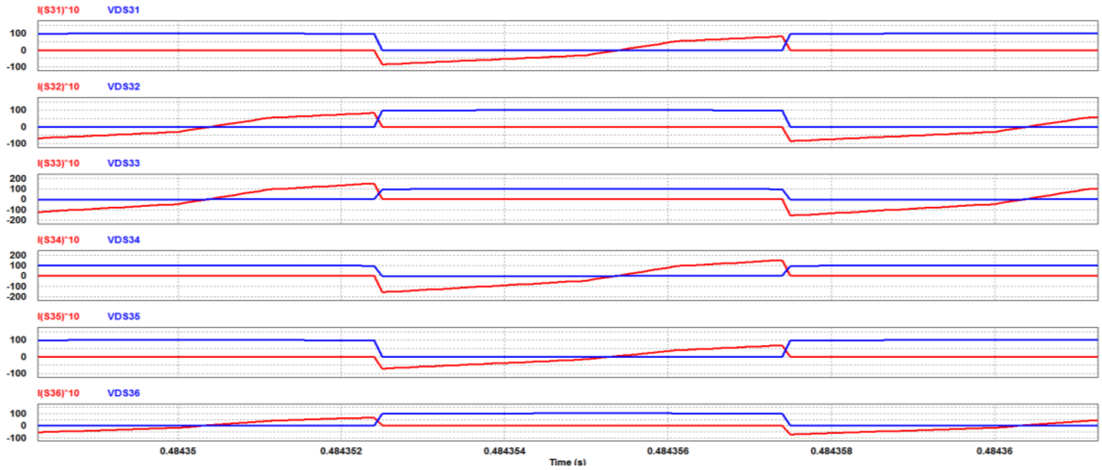

Figure 12. Switch current and voltage waveforms AB interfacing port 3, for 10% load

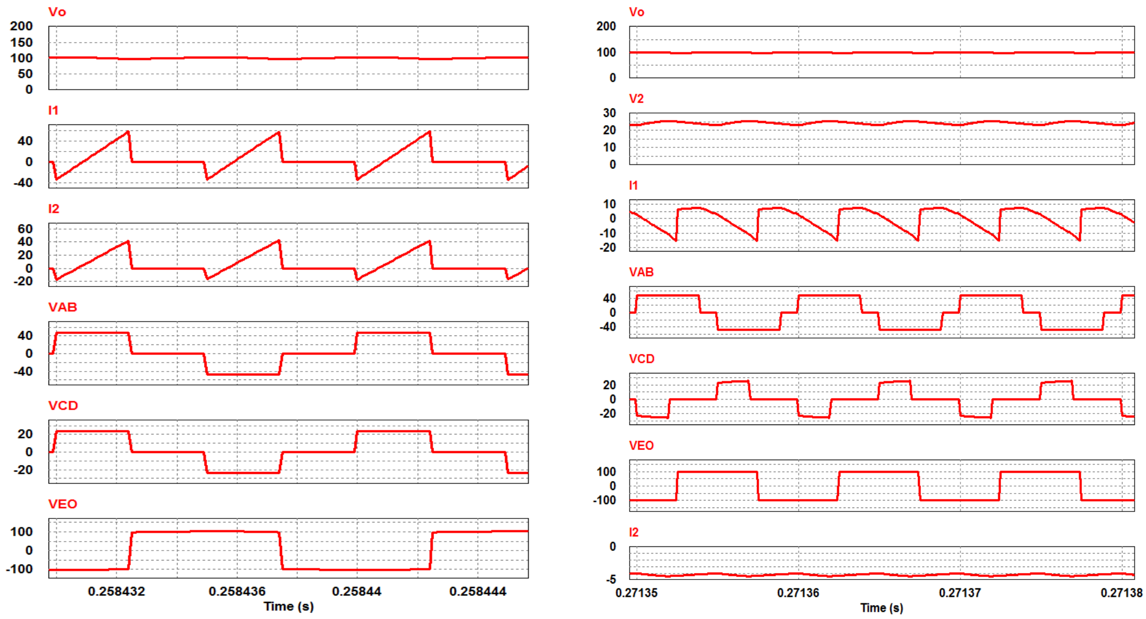

(a) (b)

Figure 13. Converter waveforms in (a) Dual input single output mode (b) Single input dual output mode

6. CONCLUSION

DTATAB topology was proposed to overcome the disadvantages of isolated TAB topology**.** Phase shift control was used for the topology. In this paper duty ratio control is proposed to increase the range of soft switching for wide variation of load power as well as the source port voltage. Duty ratios D_1 and D_2 are adjusted to regulate the load voltage V_3 and control the port powers P_1 and P_2, keeping the phase shift (ϕ_{13} and ϕ_{23}) fixed at 0.5π, for change in load or source voltage V_1 and V_2 or both. The direction of power flow P_1 can be reversed by fixing ϕ_{13} at -0.5π, P_2 can be reversed by fixing ϕ_{23} at -0.5π. The converter was designed to maximize the switch utilisation.

A 100V, 1KW ,3 port converter was simulated to verify the proposed method and it was observed that the load voltage is regulated with soft switching in all its switches for changes in the load and supply voltage.The bidirectional capability of the converter is demonstrated by loading port 2 and 3 at 100W and 500W, respectively. The load voltages at port 2 and 3 were regulated at 24V and 100V. The effectiveness of duty ratio control over phase shift controlin ZVS operation, with respect to the range of port voltage and load was mathematically demonstrated in section 3.

The proposed duty ratio control is an effective and easy way to control the magnitude and direction of the port powers in a dual transformer isolated three port converter. Since operation with ZVS is achieved for all possible values of load and source voltages, the switching losses in the converter with the proposed modulation technique will be lesser compared to other modulation techniques reported in the literature. The technique can be conveniently scaled up for increase in the number of ports. However, thepeak value of switch current decreases at a low rate for decrease in the load. Hence future work may be onreducing the peak current with reduction in load and further increase the switch utilisation.

REFERENCES

[1] A.K. Bhattacharjee, N. Kutkut and I. Batarseh, "Review of Multiport Converters for Solar and Energy Storage Integration," *IEEE Trans. Power Electron*., vol. 34, no. 2, pp. 1431–1445, Feb. 2019, DOI: 10.1109/TPEL.2018.2830788.

[2] Adarsh S. and Nagendrappa H, "Multiport Converters to Integrate Multiple Sources and Loads- A Review of Topologies," in *Proc. 2018 4th International Conference for Convergence in Technology (I2CT)*, SDMIT Ujire, Mangalore, India., Oct 27-28, pp. 1-7, 2018, DOI: 10.1109/I2CT42659.2018.9058269.

[3] S. Arulmozhi and K. R. Santha "Review of multiport isolated bidirectional converter interfacing renewable and energy storage systems," *International Journal of Power Electronics and Drives System (IJPEDS)*, vol. 11, no. 1, pp. 466-476, March 2020, DOI: 10.11591/ijpeds.v11.i1.pp466-467.

[4] O. A. Hassan, S. A. Zulkifli, M. S. Zainal, A. A. M. Radzi, M. S. Ahmad, and T. N. T. Ibrahim, "Independent high voltage DC source development for renewable grid integration interface", *International Journal of Power Electronics and Drives System (IJPEDS)*, vol. 11, no. 1, pp. 374-381, March 2020, DOI: 10.11591/ijpeds.v11.i1.pp374-381.

[5] D. Liu and H. Li, "A ZVS Bi-Directional DC–DC Converter for Multiple Energy Storage Elements," in *IEEE Transactions on Power Electronics*, vol. 21, no. 5, pp. 1513-1517, Sept. 2006, DOI: 10.1109/TPEL.2006.882450.

[6] S. A. Khan, M. R. Islam, Y. Guo, and J. Zhu, "A New Isolated Multi-Port Converter With Multi-Directional Power Flow Capabilities for Smart Electric Vehicle Charging Stations," in *IEEE Transactions on Applied Superconductivity*, vol. 29, no. 2, pp. 1-4, March 2019, DOI: 10.1109/TASC.2019.2895526.

[7] B. J. D. Vermulst, J. L. Duarte, E. A. Lomonova, and K. G. E. Wijnands, "Scalable multi-port active-bridge converters: modelling and optimised control," in *IET Power Electronics*, vol. 10, no. 1, pp. 80-91, 20 1 2017, DOI: 10.1049/iet-pel.2016.0191.

[8] L. Piris-Botalla, G. G. Oggier, and G. O. García, "Extending the power transfer capability of a three-port DC–DC converter for hybrid energy storage systems," in *IET Power Electronics*, vol. 10, no. 13, pp. 1687-1697, 27-10-2017, DOI: 10.1049/iet-pel.2016.0422.

[9] R. Liu, L. Xu, Y. Kang, Y. Hui, and Y. Li, "Decoupled TAB converter with energy storage system for HVDC power system of more electric aircraft," in *The Journal of Engineering*, vol. 2018, no. 13, pp. 593-602, 2018, DOI: 10.1049/joe.2018.0033.

[10] J. L. Duarte, M. Hendrix, and M. G. Simoes, "Three-Port Bidirectional Converter for Hybrid Fuel Cell Systems," *in IEEE Transactions on Power Electronics*, vol. 22, no. 2, pp. 480-487, March 2007, DOI: 10.1109/TPEL.2006.889928.

[11] Song, S. Li, W. Ni, K. Xu, H. Hu, Y. Si, J. "Modular Multi-Port Ultra-High Power Level Power Converter Integrated with Energy Storage for High Voltage Direct Current (HVDC) Transmission," *Energies*, 2018, DOI: 10.3390/en11102711.

[12] S. Baek and S. Bhattacharya, "Isolation Transformer for 3-Port 3-Phase Dual-Active Bridge Converters in Medium Voltage Level," in *IEEE Access*, vol. 7, pp. 19678-19687, 2019, DOI: 10.1109/ACCESS.2019.2895818.

[13] P. Purgat, S. Bandyopadhyay, Z. Qin, and P. Bauer, "Isolation Transformer for 3-Port 3-Phase Dual-Active Bridge Converters in Medium Voltage Level," in *IEEE Transactions on Power Electronics*, vol. 36, no.5, pp. 5425-5439, May 2021, DOI: 10.1109/ACCESS.2019.2895818.

[14] H. Tao, A. Kotsopoulos, J. L. Duarte, and M. A. M. Hendrix, "Transformer-Coupled Multiport ZVS Bidirectional DC–DC Converter with Wide Input Range," in *IEEE Transactions on Power Electronics*, vol. 23, no. 2, pp. 771-781, March 2008, DOI: 10.1109/TPEL.2007.915129.

[15] H. Tao, J. L. Duarte, and M. A. M. Hendrix, "Three-Port Triple-Half-Bridge Bidirectional Converter with Zero-Voltage Switching," in *IEEE Transactions on Power Electronics*, vol. 23, no. 2, pp. 782-792, March 2008, DOI: 10.1109/TPEL.2007.915023.

[16] L. Wang, Z. Wang, and H. Li, "Asymmetrical Duty Cycle Control and Decoupled Power Flow Design of a Three-port Bidirectional DC-DC Converter for Fuel Cell Vehicle Application," in *IEEE Transactions on Power Electronics*, vol. 27, no. 2, pp. 891-904, Feb. 2012, DOI: 10.1109/TPEL.2011.2160405.

[17] Ajami and P. AsadiShayan, "Soft switching method for multiport DC/DC converters applicable in grid connected clean energy sources," in *IET Power Electronics*, vol. 8, no. 7, pp. 1246-1254, 7 2015, DOI: 10.1049/iet-pel.2014.0592.

[18] Zhao, S. D. Round, and J. W. Kolar, "An Isolated Three-Port Bidirectional DC-DC Converter with Decoupled Power Flow Management," in *IEEE Transactions on Power Electronics*, vol. 23, no. 5, pp. 2443-2453, Sept. 2008, DOI: 10.1109/TPEL.2008.2002056.

[19] S. Falcones, R. Ayyanar, and X. Mao, "A DC–DC Multiport-Converter-Based Solid-State Transformer Integrating Distributed Generation and Storage," in *IEEE Transactions on Power Electronics*, vol. 28, no. 5, pp. 2192-2203, May 2013, DOI: 10.1109/TPEL.2012.2215965.

[20] G. Buticchi, L. F. Costa, D. Barater, M. Liserre, and E. D. Amarillo, “A Quadruple Active Bridge Converter for the Storage Integration on the More Electric Aircraft,” in *IEEE Transactions on Power Electronics*, vol. 33, no. 9, pp. 8174-8186, Sept. 2018, DOI: 10.1109/TPEL.2017.2781258.

[21] M. Rashidi, N. N. Altin, S. S. Ozdemir, A. Bani-Ahmed, and A. Nasiri, “Design and Development of a High-Frequency Multiport Solid-State Transformer with Decoupled Control Scheme,” in *IEEE Transactions on Industry Applications*, vol. 55, no. 6, pp. 7515-7526, Nov.-Dec. 2019, DOI: 10.1109/TIA.2019.2939741.

[22] H. Krishnaswami and N. Mohan, “Three-Port Series-Resonant DC-DC Converter to Interface Renewable Energy Sources with Bidirectional Load and Energy Storage Ports,” in *IEEE Transactions on Power Electronics*, vol. 24, no. 10, pp. 2289-2297, Oct. 2009, DOI: 10.1109/TPEL.2009.2022756.

[23] L. Hang, B. Li, S. Liu, Y. Gu, W. Yao, and Z. Lu, “Asymmetrical secondary structure of LLC series resonant DC/DC converter for multi-output applications,” in *IET Power Electronics*, vol. 4, no. 9, pp. 993-1001, November 2011, DOI: 10.1049/iet-pel.2010.0146.

[24] Y. Wang, F. Han, L. Yang, R. Xu, and R. Liu, “A Three-Port Bidirectional Multi-Element Resonant Converter with Decoupled Power Flow Management for Hybrid Energy Storage Systems,” in *IEEE Access*, vol. 6, pp. 61331-61341, 2018, DOI: 10.1109/ACCESS.2018.2872683.

[25] M. Phattanasak, R. Gavagsaz-Ghoachani, J. Martin, B. Nahid-Mobarakeh, S. Pierfederici, and B. Davat, “Control of a Hybrid Energy Source Comprising a Fuel Cell and Two Storage Devices Using Isolated Three-Port Bidirectional DC-DC Converters,” in *IEEE Transactions on Industry Applications*, vol. 51, no. 1, pp. 491-497, Jan.-Feb. 2015, DOI: 10.1109/TIA.2014.2336975.

[26] Z. Zhang, O. C. Thomsen, M. A. E. Andersen, and H. R. Nielsen, “Dual-input isolated full-bridge boost DC-DC converter based on the distributed transformers,” in *IET Power Electronics*, vol. 5, no. 7, pp. 1074-1083, August 2012, DOI: 10.1049/iet-pel.2011.0181.

[27] D. Gunasekaran and L. Umanand, “Integrated magnetics based multi-port bidirectional DC-DC converter topology for discontinuous-mode operation,” in *IET Power Electronics*, vol. 5, no. 7, pp. 935-944, August 2012, DOI: 10.1049/iet-pel.2011.0492.

[28] V. N. S. R. Jakka, A. Shukla, and G. D. Demetriades, “Dual-Transformer-Based Asymmetrical Triple-Port Active Bridge (DT-ATAB) Isolated DC-DC Converter,” in *IEEE Transactions on Industrial Electronics*, vol. 64, no. 6, pp. 4549-4560, June 2017, DOI: 10.1109/TIE.2017.2674586.

[29] E. Asa, K. Colak, M. Bojarski and D. Czarkowski, “Asymmetrical Duty-Cycle and Phase-Shift Control of a Novel Multiport CLL Resonant Converter,” in *IEEE Journal of Emerging and Selected Topics in Power Electronics*, vol. 3, no. 4, pp. 1122-1131, Dec. 2015, DOI: 10.1109/JESTPE.2015.2408565.

BIOGRAPHIES OF AUTHORS

Adarsh S. was born in 1988. He received the B. E. degree in electrical & electronics engineering in 2010 form National Institute of Engineering, Mysore, India and M.Tech. degree in power electronics in 2013 from Manipal Institute of Technology, Manipal, India. He worked as an assistant manager from 2010 to 2011 in Vedanta Aluminium Limited, Orissa, India. Since 2013, he has been working as assistant professor in the department of electrical engineering, Manipal Institute of Technology, Manipal. He is on sabbatical currently to pursue PhD, in the department of electrical and electronics engineering, NITK Surathkal. He is interested in working on high frequency Multiport and Bidirectional DC-DC converters applied to renewable energy sources.

NagendrappaHarischandrappa was born in the village Nakaralathanda, Bellary, India in 1977. He received the B. E. degree in electrical & electronics engineering in 1999, M.Tech. degree in power and energy systems in 2002 both from the National Institute of Technology Karnataka (NITK), Surathkal, India and, the Ph.D. degree in electrical engineering in 2015 from the University of Victoria, Victoria, British Columbia, Canada. He worked as an assistant lecturer from 2002 to 2004, and as a teaching fellow from 2004 to 2006 both in the department ofelectrical engineering, NITK Surathkal. For a short period he worked as an assistant engineer (operation and maintenance) in the power distribution utility called Mangalore electricity supply company (MESCOM) Ltd. at Ajjampura, Tarikere, India. Since 2006, he has been working as assistant professor in the department of electrical engineering, NITK Surathkal. He is interested in working on high frequency soft-switching converters for power generation fromrenewable energy sources and their grid interfacing applications.